Check for updates

Enhanced removal of emerging contaminants from tap water by developing graphene oxide and nanoplatelet hybrid aerogels†

G. Gorgolis, [ID] *[ab] F. Tunioli,[c] G. Paterakis,[ab] M. Melucci, [ID] *[c] N. Koutroumanis,[b] L. Sygellou, [ID] [b] M. S. S. Bafqi,[d] B. Saner Okan*[de] and C. Galiotis [ID] *[ab]

The removal of emerging contaminants (ECs) from drinking water is a current challenge of global concern. Graphene-based sorbents are attracting increasing interest in this field owing to the chemical versatility of graphene-based materials, their commercial availability and processability in various 3D structures. Herein, for the first time, graphene aerogels (GAs) are reported based on the synergy of graphene oxide (GO) and graphene nanoplatelets (GNPs) derived from waste tire and their use as a sorbent for a mixture of ECs in tap water. Reduction of GO up to 52.1% (O/C = 0.092) was demonstrated through X-ray photoelectron spectroscopy, whereas no changes in the GNP structure during aerogel synthesis were demonstrated with comprehensive spectroscopic and microscopic characterisation. Adsorption of a selection of ECs in a mixture from tap water was tested under flow conditions by inserting the aerogels into filtration cartridges and filtering tap water spiked with the mixture of ECs. Remarkably, the GO + GNP aerogel showed an increase in adsorption capacity of about 2.3 times that of the rGO aerogel owing to the higher obtained surface area, 27 instead of 16 m^2 g^{-1}, and the resultant more-reduced structure.

1. Introduction

Drinking-water purification is one of the major challenges of the years to come. Increasing cases of contamination with emerging contaminants (ECs)[1,2] urgently call for the development of advanced materials and purification technologies. Many of these contaminants end up in surface- and groundwater and have even been detected in EU drinking water. Directive EU 2020/2184 has introduced new limits and, in some cases, tightened existing values for already regulated contaminants.[3] Additionally, this directive requires water operators to conduct risk assessment and develop water safety plans to address these risks. Overall, this is pushing joint industrial and academic efforts to develop new technologies that can remove

ECs at sustainable costs to replace state-of-the-art technology mainly relying on multistep treatments, including activated carbon adsorption and membrane filtration.[4,5]

Nanomaterials, with their tunable multifunctionalities, are attracting growing interest in realizing three-dimensional (3D) structures such as aerogels and membranes for adsorption and/or filtration purposes.[6,7] Graphene, owing to its unique surface properties and processability, is expected to lead major advances in the drinking water purification field by producing innovative materials with higher removal capacity for a wider range of contaminants.[8,9] In particular, graphene oxide (GO) and its derivatives have shown promising adsorption properties toward several ECs, including drugs and dyes.[10–12] GO nanosheets and graphene nanoplatelets (GNPs) can be used as powder sorbents in dispersion if coupled with a further purification step such as micro- or ultrafiltration, allowing the retention of the emerging contaminants at the carbon nanomaterials by the filter cutoff.[11,13] Alternatively, 3D graphene-based structures, including membranes and composite hydrogels or aerogels, have been proposed as sorbent materials to be used as a single step of purification.[9,14–17] The advantage in the latter case is the ease of use of 3D structures and the possibility of their reuse after extraction and washing-regeneration, as well as their high surface area, which promotes adsorption properties.[9,18–20]

Graphene aerogels (GAs) can be produced using different methods, leading to materials with remarkable properties such as very low density; high electrical conductivity; high

[a]Faculty of Chemical Engineering – University of Patras, Panepistimioupoli, 26504 Rio, Achaia, Greece. E-mail: galiotis@chemeng.upatras.gr; manuela.melucci@isof.cnr.it; ggorgolis@upatras.gr

[b]Foundation of Research and Technology – Institute of Chemical Engineering Sciences, Stadiou Str., Platani – 26504, Greece

[c]Institute for Organic Synthesis and Photoreactivity (ISOF), National Research Council of Italy (CNR), Via P. Gobetti 101, I-40129 Bologna, Italy

[d]Sabanci University Integrated Manufacturing Technologies Research and Application Center & Composite Technologies Center of Excellence, Teknopark Istanbul, Pendik, 34906, Istanbul, Turkiye. E-mail: burcu.saner@sabanciuniv.edu

[e]Faculty of Engineering and Natural Sciences, Materials Science and Nanoengineering, Sabanci University, Tuzla, 34956, Istanbul, Turkiye

† Electronic supplementary information (ESI) available. See DOI: https://doi.org/10.1039/d4ra05658b
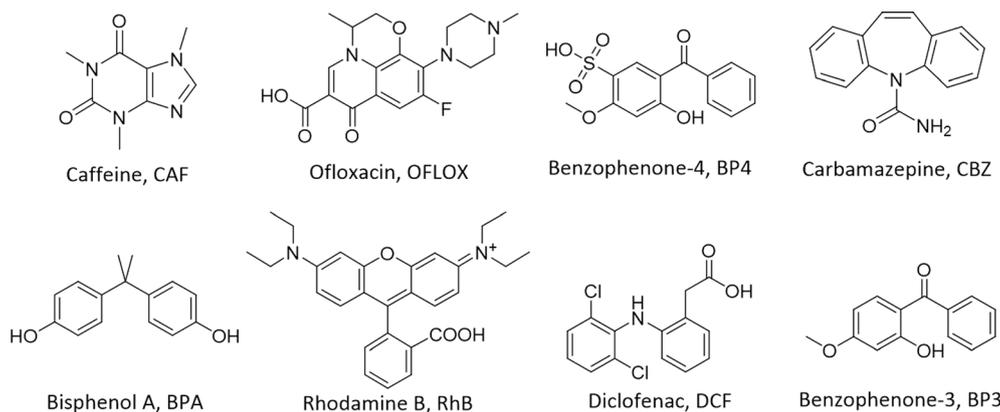
Fig. 1 Chemical structure of the water organic contaminants selected for the adsorption test.

mechanical strength; thermal stability and high adsorption capacity for dyes, oils, organic solvents and inorganic ions.[21,22] Consequently, GAs can be exploited in several applications, such as electrodes for electrochemical power sources and lithium-ion batteries, as supercapacitors, in air purification, in the removal of several oils and dyes from water, and generally in wastewater management.[23–26]

In this scenario, the successful synthesis and applications of graphene oxide (GO) and graphene nanoplatelets (GNPs)-biopolymer (chitosan, alginates) aerogels for the adsorption of several organic molecules and a heavy metal (lead Pb^{2+}) from tap water have been recently reported by some of the co-authors.[9,27] GO-doped 3D chitosan–gelatin aerogels showed a maximum adsorption capacity of 11.1 mg g^{-1} for lead. The adsorption capacity for fluoroquinolonic antibiotics (ofloxacin and ciprofloxacin) was found to be equal to 5–8 mg g^{-1}, while no adsorption was found for the chitosan–gelatin aerogels without GO. For graphene–alginate hydrogels, the removal of a mixture of eight selected ECs in tap water, including bisphenol A, ofloxacin and diclofenac, was assessed. Rhodamine B was found to be efficiently adsorbed (178 mg g^{-1}), while the regeneration capability was investigated by washing with ethanol, with high adsorption performance up to the fourth reuse cycle.[9] Han *et al.* have created graphene nanoplatelets (GNPs)/boron nitride (BN) aerogels as adsorbents for the removal of pharmaceutical ciprofloxacin from its aqueous solutions demonstrating the synergy of the two two-dimensional materials.[28] Pure graphene-based aerogels[23–26] have also been reported for organic dye pollutant removal. Sun *et al.* have prepared GAs using this technique and demonstrated the contaminant removal by using methylene blue (MB) as a precursor.[29] The adsorption quantity can reach 87.30 mg g^{-1}, while the removal rate was found to be equal to 95.1%. It was claimed that the sorption process may invoke electrostatic attraction, ion exchange, surface complexation and π–π stacking mechanisms. Also, Trinh *et al.* have reported GAs with ethylenediamine as the reducing agent.[30] The maximum adsorption capacity of this neat GA for MB was calculated to be equal to 221.77 mg g^{-1}.

In this work, the synthesis of GAs prepared from a mixture of GO and sustainable graphene nanoplatelet GNPs deriving

from waste tires[9] is reported. Spectroscopic and microscopic characterisation with the assistance of X-ray photoelectron spectroscopy (XPS), scanning electron microscopy (SEM), X-ray diffraction (XRD) and Raman spectroscopy confirmed the partial reduction of GO, whereas the GNPs structure remained intact. The aerogels were exploited to adsorb a mixture of eight ECs (Fig. 1) from tap water in dynamic conditions (*i.e.*, contact time of second), and the selectivity and removal capacity were studied to attain the highest adsorption with a suitable material system. To the best of the authors' knowledge, this hybrid graphene aerogel (GO + GNPs) structure behaves differently in terms of adsorption capacity compared to the previously designed neat reduced GO (rGO) aerogel.[24–26,31] The higher obtained surface area and the more efficient reduction of GO in the first case are believed to result in superior performance.

2. Experimental procedure

2.1 Graphene oxide preparation

The graphene oxide (GO) is synthesised from natural graphite flakes (NGS Naturgraphit GmbH, Germany) by a two-step oxidation process based on a method, which is a modification of Hummer's method,[32,33] namely, a pre-oxidation step at the beginning, followed by the final oxidation step where GO flakes are collected in aqueous dispersion (analytical information can be found in the ESI file†).

2.2 Synthesis of oxidised GNPs

GNPs were oxidised in order to be grafted with oxygen groups and combined efficiently with GO into an aqueous precursor solution that afterwards turns into an aerogel (as described following). The oxidation was achieved using sulfuric acid (H_2SO_4, 97%) and potassium permanganate ($KMnO_4$).[34] Initially, 3 g of GNPs were added in a flask with 70 mL of H_4SO_4 at 20 °C in a water bath. Gradually, 26.7 g potassium permanganate ($KMnO_4$) was added to the mixture. Thereafter, the mixture was heated to 40 °C for 2 h, where 50 mL of DW was added carefully. After 15 minutes, the reaction was terminated by adding 500 mL of DW and 7 mL of hydrogen peroxide (H_2O_2,

30%). Finally, the mixture was washed with a 1 : 10 HCl solution to remove most of the metal ions and subjected to dialysis until the pH was neutralized.

2.3 Synthesis of GNPs from waste tires

Graphene nanoplatelets (GNPs) were synthesized from the pyrolyzed carbon black obtained from waste tires by the purification, catalytic activation and heat treatment process. Within this process, the waste tires are shredded and cut into four main pieces prior to thermal decomposition. The tire shreds are then pyrolyzed at temperatures of 400 °C in a batch reactor under a nitrogen atmosphere to produce carbon black. Then, the carbon black was treated in mild conditions without using harsh chemicals (sulphuric acid and nitric acid) to decrease inorganic impurities as well as remove undesirable (ash) contents. In the final stage, metal impregnation was performed on a known weight of the treated carbon black, and then the material was placed in a furnace for catalytic carbonization, which resulted in the formation of the graphene nanoplatelets.[35]

2.4 Graphene aerogel synthesis

The prepared GO was combined with the GNPs powder after further oxidation of the latter. Substantially, a synergy of the two graphene-oxide formulations took place to obtain the graphene aerogels. The approach presented previously by Hong et al.[36] was followed herein for the synthesis of the reduced graphene oxide (rGO) aerogels. The aqueous solution of GO consisted of both starting materials (GO and oxidised GNPs, with an analogy 50/50% w/w), and after its preparation, it was subsequently diluted in water to obtain a concentration of 1 mg mL^{-1}. Hypophosphorous acid (H_3PO_2) and iodine (I_2) of weight ratio $GO : H_3PO_2 : I_2$ 1 : 100 : 10, were then added as the chemical reducing agents. Subsequently, the solution was placed in a furnace and heated to 80 °C for 8 hours, resulting in a uniform gelation of the GO. The sample was then rinsed with water until a pH equal to 7, followed by freeze-drying for 48 h. The chemical reaction that relates to the chemical reduction of graphene oxide has both H_3PO_2 and I_2 as reactants. Based on the proposed self-assembly mechanism of the graphene sheets,[37] at first, H_3PO_2 combines with I_2 and creates hydriodic acid that acts as the reducing agent and is responsible for the pH decrease of the medium (pH < 1). The decreased value of pH results in diminished electrostatic repulsions, aiding the formation of GO agglomerates. The oxygen-containing functional groups on the GO surface are reduced from hydriodic acid and produce chemically converted graphene. With the aim of creating a more stable structure, the rinsed hydrogel was pre-frozen in a refrigerator (−27 °C) for up to a week until the freeze-drying took place (Fig. S1†).

2.5 Structural characterisation methods

SEM photos were taken using a LEO SUPRA 35 VP and FE-SEM (FEI InspectTM F50) using the SE detector. The signal by the backscattered electrons is collected by the SE detector and has been converted to a signal that is sent to a computer for further analysis. The samples were sputter-coated with gold for examination under SEM. The Raman spectra of the specimens were recorded using an InVia Reflex (Renishaw, UK) Micro-Raman equipment using a 633 nm laser excitation. In all experiments, spectra were recorded at several points on each specimen using a Renishaw InVia Raman Spectrometer with a 1200 groove per mm grating and an ×100 lens. The power of the laser beam was kept below 1 mW to avoid heating the specimen. Raman spectra were baseline-corrected, and graphene peaks were fitted to Lorentzian functions. When graphene peaks were superimposed onto the peaks of the substrates, the necessary deconvolution process was applied. In this analysis, the Lorentzian components assigned to the substrates were held fixed, with their parameters (position: full-width at half-maximum) evaluated from the spectra of the bare substrates. X-ray diffraction measurements were performed with the assistance of a Bruker D8 Advance model diffractometer.

The surface analysis measurements were performed in a UHV chamber (P∼5 × 10^{-10} mbar) equipped with a SPECS Phoibos 100-1D-DLD hemispherical electron analyser and a non-monochromatized dual-anode Mg/Al X-ray source for XPS. The XP Spectra were recorded with MgKa at 1253.6 eV photon energy and an analyser pass energy of 15 eV, giving a full width at half maximum (FWHM) of 0.85 eV for the Ag 3d$_{5/2}$ line. The analysed area was a spot with a diameter of 3 mm. The atomic ratios were calculated from the intensity (peak area) of the XPS peaks weighted with the corresponding relative sensitivity factors (RSF) and the energy analyser transmission function. For spectra collection and treatment, including fitting, the commercial software SpecsLab Prodigy (by Specs GmbH, Berlin) was used. The XPS peaks were deconvoluted with a sum of Gaussian–Lorentzian peaks after Shirley-type background subtraction.

Specific surface area and porosity measurements were performed by obtaining the volumetric nitrogen adsorption at 78 K using an "autosorb iQ Model 7" gas sorption system and high purity gases (>99.999%). Before the measurement, the as-formed aerogel was outgassed at 150 °C under vacuum (P < 10^{-5} mbar) for 10 hours. The specific surface area was found following the multi-point BET equation. The pore volume was calculated from the adsorbed nitrogen at 0.90 relative pressure. The pore size distribution was determined with the Barrett–Joyner–Halenda (BJH) model.[38]

2.6 Adsorption test

Aerogels were placed inside a column (SepaChrom Purezza) and blocked by frit, and they were kept overnight in water to hydrate and used under flow conditions. A mixture of eight organic contaminants (0.5 mg L^{-1} each in tap water) was prepared and then made to flow by a peristaltic pump through the cartridge (flow rate 2.5 mL min^{-1}). Samples were collected every 20 mL, and the output concentration was measured by HPLC. All tests were carried out in duplicate and reported as mean values with standard deviation.

2.6.1 High-performance liquid chromatography analyses.
HPLC analyses of the selected mixture of eight contaminants were performed on a Dyonex Ultimate 3000 system equipped with

a diode array detector. 200 μL of samples were used as sources for the automated injection. The chromatographic separation was performed on a reverse phase Zorbax XDB-C8 column (4.6 × 150 mm^2, 5 μm) at a flow rate of 1.0 mL min^{-1}, detection at λ_{max} of each analyte, and linear gradient TFA 0.05% aqueous solution/acetonitrile from 80 : 20 to 0 : 100. In each experiment, the removal of each analyte was determined by comparison with that of the initial untreated solution. The results are expressed as the mean of two independent experiments ±SD.

3. Results and discussion

3.1 Structural aspects of graphene aerogels

The starting GNPs powder and the as-prepared graphene aerogels were characterised by combined Raman spectroscopy, XRD, SEM and XPS analyses. XPS was carried out in order to gain an insight into the elemental composition and chemical bonding of the starting and the resultant materials. From the XPS analysis of the neat GNPs powder and the peak intensities of C 1s, O 1s, Fe 2p$_{3/2}$ and Si 2p, the % relative atomic ratio can be extracted, and the results are shown in Table S1.† The % component concentration was calculated for C : O and found to be equal to 93.5 : 5.5. Moreover, traces of Fe and Si were detected. From the XRD diagrams of the ESI file (Fig. S6),† the main conclusion is that the product from the pyrolysis of car tires mainly consists of graphite since a clear and sharp peak at 26° is

shown, characteristic of the graphitic (002) plane.[24,39,40] The presence of graphene cannot be argued since a broad peak is not observed. Also, the presence of silicon is indeed revealed for both batches of the starting material. Specifically for the first batch, the peaks at ≈50°, 54° and 57.5° are attributed to silicon (Si),[41] while for the second one, the corresponding peaks are located at 28°, 47.5°, 54° and 57.5°. Other main peaks detected at 33° and 36–37° are characteristic of the existing iron (Fe).[41] From the adopted Raman spectroscopy and Fig. S7,† it is shown that the commercial graphene powder consists of graphite nanosheets. In fact, the characteristic asymmetric shape of the 2D peak suggests that the nanosheets are composed of approximately 10 graphene layers.[42,43] The G peak position appears at 1600 cm^{-1}, whereas the D peak is quite intense, revealing the existence of crystal edges and structural defects.[44]

The deconvoluted XPS C 1s spectrum of the as-resultant GO + GNPs aerogel is shown in Fig. 2A. The peak is classified into five components at binding energies (BE): (1) 284.4 ± 0.1 eV assigned to C–C sp^2 hybridization, (2) 285.3 ± 0.1 eV assigned to C–C sp^3 hybridization, (3) 286.3 ± 0.1 eV assigned to epoxides and/or hydroxides (C–O(H)), (4) 288.0 ± 0.1 eV assigned to carbonyls (C=O) and (5) 289.0 ± 0.1 eV assigned to carboxyls.[45] The deconvoluted XPS O 1s spectrum is shown in the ESI file† and classified into two components at binding energies of 531.3 ± 0.1 eV and 533.2 ± 0.2 eV assigned to C=O and C–O bonds, respectively.[32] The SEM image of the GO + GNPs aerogel is given
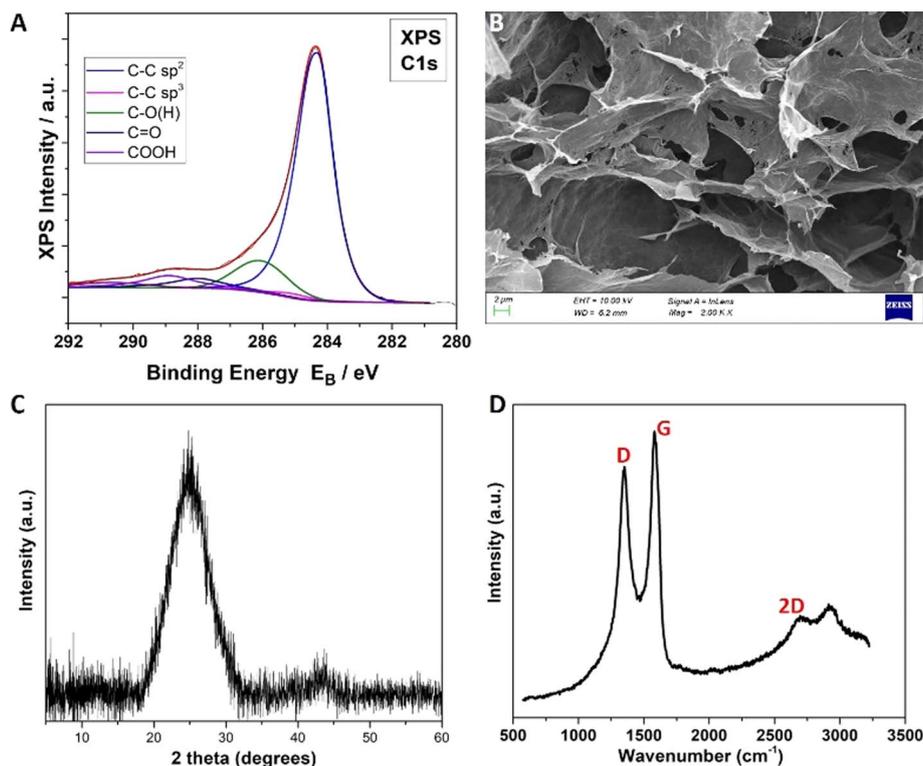

Fig. 2 Characterisation of the GO + GNPs aerogels. (A) Deconvoluted C1s XPS spectrum of the GO + GNP aerogel. (B) SEM photo of the as-obtained graphene aerogel showing the macro-porosity of the material. (C) XRD diagram of the aerogel. The as-made graphene aerogel exhibits a weak broad peak, characteristic of an amorphous material, at $2\theta = 26°$, which corresponds to the (002) plane of the graphite structure. (D) Raman spectrum of the aerogel showing the characteristic G, D and 2D peaks of graphene.

Table 1 % C 1s and O 1s component concentrations derived from the C 1s and O 1s peak deconvolution (Fig. 2), respectively, and the relative atomic ratio for the GO + GNP aerogel (C : O : P)

% Component of O bonds		% Component of C bonds					% Relative atomic ratio
C–O	C=O	C–C sp^2	C–C sp^3	C–O(H)	C=O	COOH	C : O : P
63.3	36.7	74.4	2.0	11.7	5.5	6.5	77.9 : 18.0 : 4.1
							C/O = 77.9/6.0 = 13.0

in Fig. 2B. As shown, the rGO layers have created a robust macro-scale porous network since the aerogels have been formed. In Fig. 2C and D, XRD and Raman measurements are shown for the GAs samples. Both the Raman and XRD measurements prove the reduction of GO to rGO in these aerogels. The XRD plot shows a broad peak at $2\theta = 26°$, which corresponds to the (002) plane of the graphite structure, as reported elsewhere.[24] The position of the Raman peaks for the GO are ~1590 cm^{-1} and 1356 cm^{-1}, corresponding to the G and D phonons, respectively (Table 1).

3.2 Adsorption capability of the developed graphene aerogels

Regarding the N$_2$ adsorption–desorption experiments, the specific surface area (SSA) of the GO + GNPs aerogel that was examined herein was calculated using the analysis software of the gas sorption system and found to be equal to 27 ($\pm$0.2) m^2 g^{-1}, which is relatively low for a graphene aerogel[36] but similar values have been reported elsewhere for related materials.[46,47] The pore volume at $p/p^0 = 0.90$ was found to be equal to 0.320 cm^3 g^{-1}. The SSA could be enhanced by using more concentrated GO starting solutions,[48] as in the present case, the concentration was equal to just 1 mg mL^{-1}. The nitrogen adsorption–desorption isotherms, actually, are more useful for porosities up to 50 nm or more, and for this range, the as-prepared aerogel exhibits low porosity. Certainly, the majority of the existing pores within the aerogel are in the range of

Table 2 Pore characteristics (volume and surface area) for corresponding pore diameters

Diameter (nm)	Pore volume (cm^3 g^{-1})	Pore surface area (m^2 g^{-1})
3.1827	0.00173	2.1764
3.5721	0.00374	4.4207
4.0274	0.00538	6.0537
4.572	0.00737	7.7917
5.2425	0.00922	9.2021
6.0928	0.0116	10.77
7.2249	0.01379	11.978
8.8378	0.01698	13.422
11.417	0.02192	15.153
16.5342	0.0319	17.568
25.8787	0.05223	20.711
79.3465	0.0735	21.783
162.3338	0.07478	21.814

micrometers, as already shown in the corresponding SEM image. Based on the shape of the aerogel's nitrogen adsorption–desorption isotherm (Fig. 3A), it is concluded that the material shows a Type II isotherm with a Type H3 hysteresis loop, according to IUPAC classification.[49] The pore network mainly consisted of macropores, which are not completely filled with pore condensates. This finding is in agreement with the SEM images, which clearly show the existence of a macropore network. Additionally, from the pore size distribution of Fig. 3B,
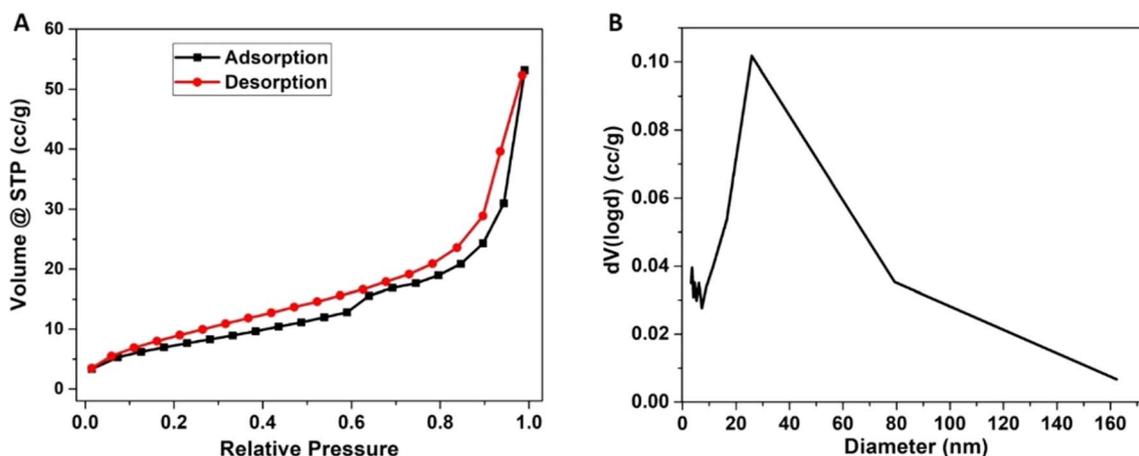

Fig. 3 (A) Pore characterisation of the GO + GNP aerogel. The nitrogen adsorption–desorption isotherm of the aerogel is shown. The BET surface area and nitrogen adsorption–desorption isotherms were measured using the analysis program of the micropore physio-/chemisorption analyser. (B) Barrett–Joyner–Halenda (BJH) pore size distribution curve of the examined aerogel.
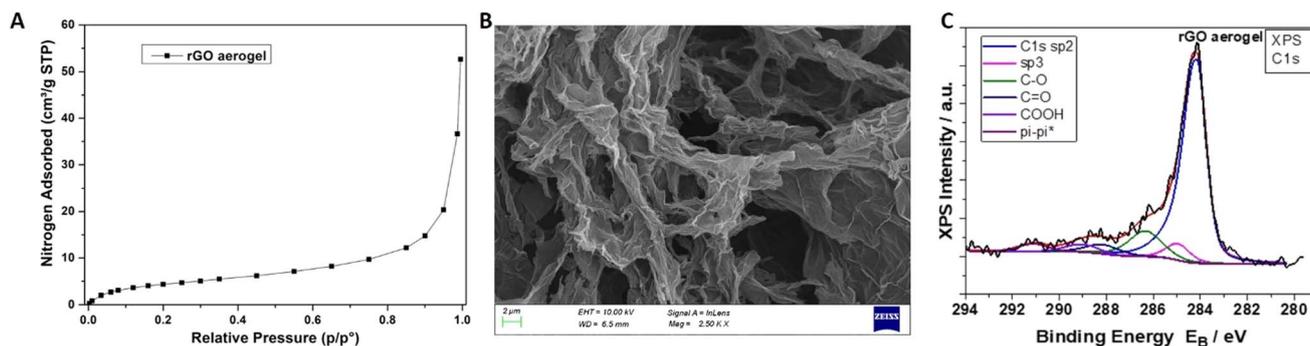
Fig. 4 (A) Nitrogen adsorption isotherm, (B) SEM image and (C) deconvoluted C 1s XPS spectrum of a neat rGO aerogel.

Table 3 XPS data of a neat rGO aerogel: % C 1s and O 1s component concentrations derived from C 1s and O 1s peak deconvolution, respectively, and the relative atomic ratio C : O : P

| Sample | % Component of C bonds | | | | | | Relative atomic ratio |
	C–C sp^2	C–C sp^3	C–O(H)	C=O	COOH	Pi–pi*	C : O : P
rGO aerogel	68.9	5.7	12.8	5.4	4.2	3.0	1 : 0.4 : 0.12

it can be deduced that the studied aerogel is characterised by both meso-porosity (between 2 and 50 nm) and macro-porosity (>50 nm). In Table 2, the pore volume and pore surface area for the corresponding diameters are shown.

Fig. 4A exhibits the nitrogen adsorption isotherm for a neat rGO aerogel, from which the basic conclusion is that the sample shows type II isotherm according to the IUPAC classification.[49] A steep nitrogen adsorption increase at high relative pressures is recorded, indicative of nitrogen condensation in macropores and relatively big mesopores. The SSA has been found to be equal to 16.7 ($\pm$0.2) m^2 g^{-1}, while the pore volume at $p/p^0 = 0.90$ is equal to 0.023 cm^3 g^{-1}. This finding is further confirmed by the SEM image in Fig. 4B, where the existence of a macropore network is clearly obvious. From the deconvoluted XPS C 1s of Fig. 4C and by analysing the peak (Table 3), the presence of sp^2 and sp^3 hybridisation and also of oxides in the form of epoxides, hydroxides, carbonyl and carboxyl groups due to the pi–pi* transition loss peak was detected.[24] From the peak areas of the C 1s, the percentage (%) component concentration can be calculated, and from the peak intensities of C 1s, O 1s, P 2p and N 1s, the (%) relative atomic ratio can also be obtained. For the calculation of the C : O atomic ratio, the oxygen concentration due to the P$_2$O$_5$ chemical state was subtracted. A rate equal to C : O = 10.8 for the neat rGO aerogel was found, suggesting the effective reduction of GO to rGO.[32]

3.3 Adsorption performance tests of the developed graphene aerogels

The adsorption capacity of the aerogels was investigated under flow conditions on a mixture of eight organic contaminants (Fig. 1) in order to detect the selectivity and removal capacity and result in the highest adsorption with a suitable material

Table 4 Removal expressed in mg of the contaminant removed per gram of each aerogel formulation (0.5 mg L^{-1} each in tap water, $V_{tot} = 100$ mL, flow rate = 2 mL min^{-1})

| mg removed per g of material | | |
	rGO	GO + GNPs
CAF	0.14	0.65
OFLOX	0.19	0.76
BP4	0.17	0.54
CBZ	0.15	0.55
BPA	0.28	0.63
RhB	0.42	0.85
DCF	0.15	0.57
BP3	0.93	0.99
Total	2.44	5.54

system. Fig. 6 shows the experimental set-up used: the spiked tap water flow through aerogels, immobilized in a cartridge, and the treated solution was analysed by HPLC.

Fig. 7a shows the average removal obtained after 100 mL of the treated solution. rGO aerogel (blue bars) showed low removal values (12–37%) for all tested ECs with the exception of BP3, which is adsorbed at 82%. GO + GNPs aerogel (orange bars) showed increased adsorption capacity towards all ECs. This aerogel was highly selective towards CAF, OFLOX, RhB and BP3 (removal values of 58, 69, 77, and 91%, respectively) and was also effective for BP4, CBZ, BPA and DCF (48, 49, 57, and 51% respectively). The removal obtained as a function of treated volume for DCF and BP3, taken as case studies, are reported in Fig. 7b and c (all the other ECs are reported in ESI, Fig. S10†). In the case of DCF, the rGO aerogel showed low removal values and saturation that occurred after 100 mL of treated solution, while
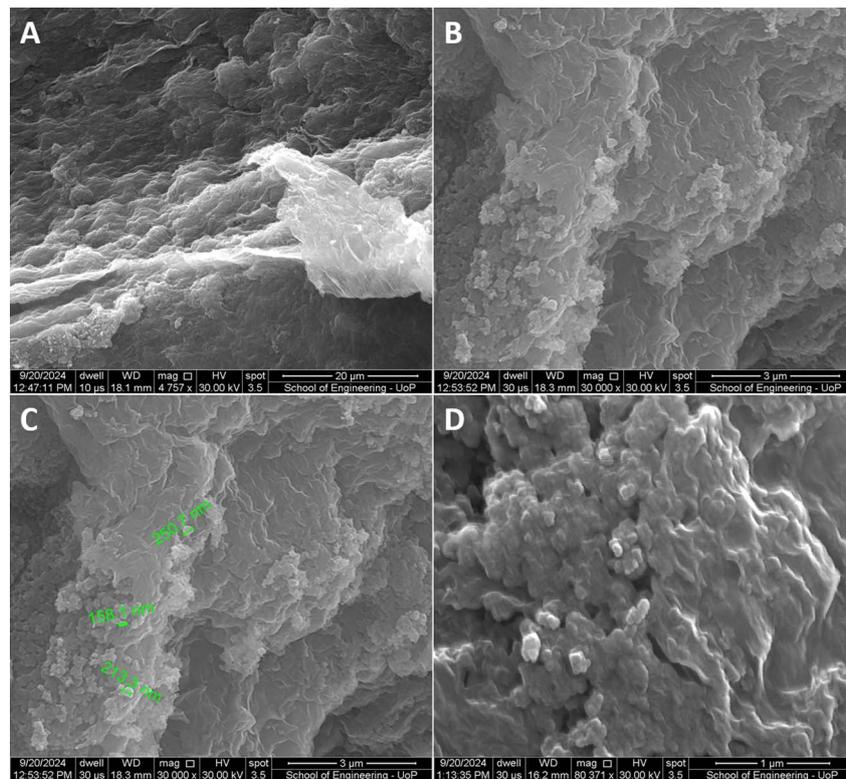
Fig. 5 Several SEM images of the as-prepared GO + GNP aerogels at different scale bars (A, B and D). In (C), the size of some GNP crystals is measured and depicted.

the GO + GNPs aerogel showed higher removal and saturation initiating after 260 mL. All other ECs (shown in Fig. S10†) showed the same trend. BP3 (Fig. 7c) is adsorbed with high removal by both aerogels, and saturation does not occur in the first 300 mL. Table 4 reports the results expressed in milligrams of the contaminant removed per gram of aerogel tested since

Fig. 6 The photographs of (a and b) the experimental set-up used to test (c) aerogels under flow conditions.

aerogels have comparable dimensions but slightly different weights. The trend observed considering the removal percentage is also confirmed by the data expressed in mg removed per g of material. GO + GNPs showed an increase in adsorption capacity of about 2.3 times the rGO (5.54 vs. 2.44 total mg removed per g of material). Remarkably, reusability test results (Fig. 7) highlight the stability of the aerogels. Indeed, the removal performance remained almost unchanged for all the selected contaminants, and there was no graphene leaching evidence (graphene is visible by baseline increase or alteration in the contaminant quantification chromatographic analyses).

The removal mechanisms in graphene-based systems are generally ascribed to hydrogen bonding,[50,51] and secondarily, the hydrophobic interactions[52] between graphene and the contaminants molecules.[9,53,54] For example, in the case of DCF, a possible occurrence of hydrogen bonding between the functional groups of the rGO aerogel and the contaminant has been suggested.[55] The N–H bending and C–N stretching from secondary amine, respectively, have been spectroscopically revealed using FTIR spectroscopy, thus confirming the attachment of the electronegative sites of DCF (N atoms) to the hydrogen atoms of rGO aerogel functional groups through the creation of hydrogen bonding.
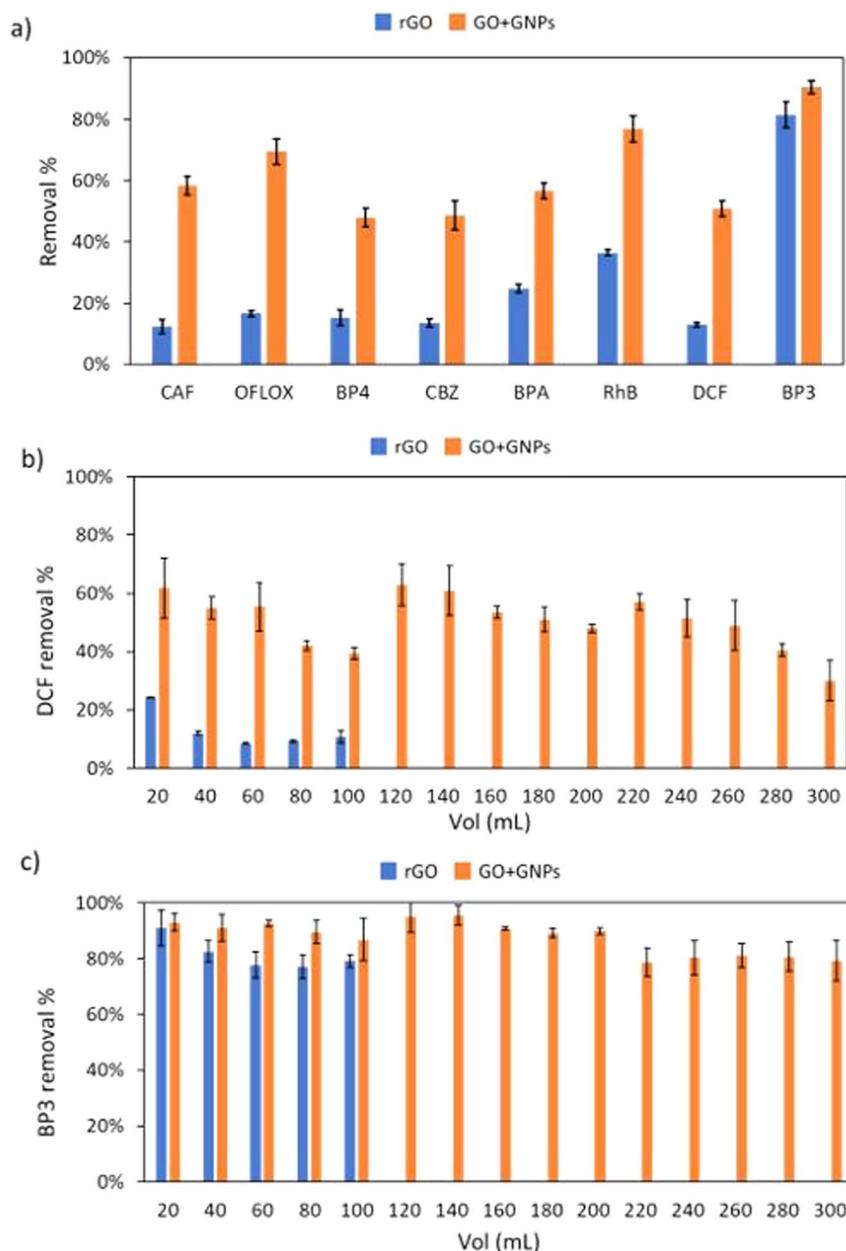

Fig. 7 (a) Average removal of a mixture of eight ECs (0.5 mg L^{-1} each in tap water, V_{tot} = 100 mL, flow rate = 2.5 mL min^{-1}) by aerogels of rGO (blue) and GO + GNPs (orange); removal of (b) diclofenac (DCF) and (c) benzophenone-3 (BP3) (0.5 mg L^{-1} each in tap water, V_{tot} = 300 mL, flow rate = 2.5 mL min^{-1}).

The superior performance of the GO + GNPs aerogel as compared to the neat rGO aerogel can be attributed to the higher obtained surface area, 27 instead of 16 m^2 g^{-1}, higher pore size, 0.320 instead of 0.023 cm^3 g^{-1} and less oxygen-groups observed in the former case. The higher surface area means that there are more active sites to interact with the ECs molecules, while the larger pore size can lead to more efficient attachment of the pollutants in the structure of the aerogel. Furthermore, the GO + GNPs formulation seems to possess a much denser structure than the neat rGO one, as also shown in the SEM images of Fig. 5. The aggregates of GNPs, the size of which is clearly shown in Fig. 5C and possibly have remained undissolved in water, may have the ability as crystals rich in carbon content to create bonding with the ECs and delay their flow in contrast to the less dense structure of the neat rGO structure. The difference in the carbon content exhibited by the two examined formulations is also believed to be significant since higher van der Waals and hydrophobic interactions between the hydrophobic regions of the material and the contaminant molecules may occur.[12]

Consequently, the better reduction and the higher surface area possessed by the GO + GNPs aerogels over the neat rGO corresponding one lead to the higher removal capability for such materials.

The adsorption results of the present study (mg removed per g of used material) are comparable to those of other similar studies. More specifically, the adsorption capacity of GO-doped 3D chitosan–gelatin aerogels for fluoroquinolonic antibiotics like ofloxacin and ciprofloxacin was found to be equal to 5–8 mg g^{-1}, while no adsorption was found for the chitosan–gelatin aerogels without GO.[27] The same mixture of eight selected emerging contaminants (ECs) in tap water was also studied in another work.[9] Alginate-GO beads, which were obtained by ionic gelation, and GNPs originating from pyrolysed waste tires were examined as adsorbers of the contaminants. It is mentioned that for RhB, both these formulations show an adsorption rate of 15 mg g^{-1}. Compared to another relative work,[56] the as-prepared aerogels of this work seem to be superior to other porous graphene structures. For the same experimental conditions (0.5 mg L^{-1}, contaminant in tap water), the adsorption of DCF is higher for the aerogels presented herein, 0.15 mg g^{-1} for the rGO aerogels and 0.57 mg g^{-1} for the GO + GNPs aerogels.

4. Conclusions

In conclusion, three-dimensional graphene aerogels have been prepared following the freeze-drying method, while graphene powder from used tire pyrolysis has also been employed and incorporated inside the solutions that in turn, lead to graphene macro-structures. A comparison of the structural features of graphene material powder with those of the aerogels shows that the reduction of graphene oxide occurs under the fabrication conditions. The aerogels were exploited to adsorb a mixture of eight ECs from tap water in dynamic conditions (i.e., contact time of second). The GO + GNPs aerogel showed an increased adsorption capacity of about 2.3 times the rGO aerogel (5.54 vs. 2.44 total mg removed per g of material). The superior performance of the GO + GNPs aerogel compared to the neat rGO aerogel can be attributed

to the higher obtained surface area, 27 instead of 16 m^2 g^{-1}, and the less oxygen group content in the first case. Collectively, this work demonstrates the ability of the three-dimensional GO + GNPs aerogels to remove the selected contaminants thanks to their composition and structure, contributing thus to the access of graphene to the water treatment market.

Data availability

The original data of the study are included in the article and its ESI material.† Further inquiries can be directed to the corresponding authors.

Conflicts of interest

There are no conflicts to declare.

Acknowledgements

References

1 G. Lofrano, O. Sacco, V. Venditto, M. Carotenuto, G. Libralato and M. Guida, et al., Occurrence and potential risks of emerging contaminants in water, Visible Light Active Structured Photocatalysts for the Removal of Emerging Contaminants: Science and Engineering, Elsevier Inc., 2020, pp. 1–25, DOI: 10.1016/B978-0-12-818334-2.00001-8.

2 N. Morin-Crini, E. Lichtfouse, G. Liu, V. Balaram, A. R. L. Ribeiro, Z. Lu, et al., Worldwide cases of water pollution by emerging contaminants: a review, Environ. Chem. Lett., 2022, 20(4), 2311–2338, DOI: 10.1007/s10311-022-01447-4.

3 European Union Council, Directive (EU) 2020/2184 of the European Parliament and of the Council of 16 December 2020 on the quality of water intended for human consumption, Off. J. Eur. Union, 2020, 1–62.

4 P. Thamarai, R. Kamalesh, A. Saravanan, P. Swaminaathan and V. C. Deivayanai, Emerging trends and promising prospects in nanotechnology for improved remediation of wastewater contaminants: Present and future outlooks, Environ. Nanotechnol. Monit. Manag., 2024, 21, 100913, DOI: 10.1016/j.enmm.2024.100913.

5 H. Azzahra, A. F. Nisaa and M. A. Mardyanto, Study on Conventional Drinking Water Treatment for Removing Emerging Contaminants: A Literature Review, *IOP Conf. Ser. Earth Environ. Sci.*, 2024, **1307**(1), 012013.

6 C. Santhosh, V. Velmurugan, G. Jacob, S. K. Jeong, A. N. Grace and A. Bhatnagar, Role of nanomaterials in water treatment applications: A review, *Chem. Eng. J.*, 2016, **306**, 1116–1137, DOI: 10.1016/j.cej.2016.08.053.

7 S. Poornima, S. Manikandan, V. Karthik, R. Balachandar, R. Subbaiya, M. Saravanan, *et al.*, Emerging nanotechnology based advanced techniques for wastewater treatment, *Chemosphere*, 2022, **303**(3), 135050, DOI: 10.1016/j.chemosphere.2022.135050.

8 F. Tunioli, T. D. Marforio, L. Favaretto, S. Mantovani, A. Pintus, A. Bianchi, *et al.*, Chemical Tailoring of β-Cyclodextrin-Graphene Oxide for Enhanced Per- and Polyfluoroalkyl Substances (PFAS) Adsorption from Drinking Water, *Chem.–Eur. J.*, 2023, **29**(60), 1–9.

9 F. Tunioli, S. Khaliha, S. Mantovani, A. Bianchi, A. Kovtun, Z. Xia, *et al.*, Adsorption of emerging contaminants by graphene related materials and their alginate composite hydrogels, *J. Environ. Chem. Eng.*, 2023, **11**(2), 109566, DOI: 10.1016/j.jece.2023.109566.

10 F. Tunioli, T. D. Marforio, L. Favaretto, S. Mantovani, V. Palermo and M. Calvaresi, Chemical Tailoring of β-Cyclodextrin-Graphene Oxide for Enhanced Per- and Polyfluoroalkyl Substances (PFAS) Adsorption from Drinking Water, *Chem.–Eur. J.*, 2023, e202301854.

11 S. Khaliha, A. Bianchi, A. Kovtun, F. Tunioli, A. Boschi, M. Zambianchi, *et al.*, Graphene oxide nanosheets for drinking water purification by tandem adsorption and microfiltration, *Sep. Purif. Technol.*, 2022, **300**, 121826, DOI: 10.1016/j.seppur.2022.121826.

12 V. Palermo, M. Calvaresi and M. Melucci, *Environ. Sci.*, 2023, **9**(4), 985–1256.

13 S. Khaliha, T. D. Marforio, A. Kovtun, S. Mantovani, A. Bianchi, N. M. Luisa, *et al.*, Defective graphene nanosheets for drinking water purification: Adsorption mechanism, performance, and recovery, *FlatChem*, 2021, **29**, 100283, DOI: 10.1016/j.flatc.2021.100283.

14 M. Zambianchi, M. Durso, A. Liscio, E. Treossi, C. Bettini, M. L. Capobianco, *et al.*, Graphene oxide doped polysulfone membrane adsorbers for the removal of organic contaminants from water, *Chem. Eng. J.*, 2017, **326**, 130–140, DOI: 10.1016/j.cej.2017.05.143.

15 F. Pinelli, T. Nespoli and F. Rossi, Graphene oxide-chitosan aerogels: Synthesis, characterization, and use as adsorbent material for water contaminants, *Gels*, 2021, **7**(4), 149.

16 A. Bessa, B. Henriques, G. Gonçalves, G. Irurueta, E. Pereira and P. A. A. P. Marques, Graphene oxide/polyethyleneimine aerogel for high-performance mercury sorption from natural waters, *Chem. Eng. J.*, 2020, **398**, 125587, DOI: 10.1016/j.cej.2020.125587.

17 R. Castaldo, R. Avolio, M. Cocca, M. E. Errico, M. Lavorgna, J. Šalplachta, *et al.*, Hierarchically porous hydrogels and aerogels based on reduced graphene oxide, montmorillonite and hyper-crosslinked resins for water and air remediation, *Chem. Eng. J.*, 2022, **430**, 133162.

18 X. Tang, S. Xia, Q. Luo, J. Liu, H. Gong, Y. Deng, *et al.*, Hierarchically Porous Graphene Aerogels with Abundant Oxygenated Groups for High-Energy-Density Surpercapacitors, *Energy Fuel.*, 2022, **36**(23), 14433–14441.

19 X. Zhang, J. Zhou, Y. Zheng, H. Wei and Z. Su, Graphene-based hybrid aerogels for energy and environmental applications, *Chem. Eng. J.*, 2021, **420**(P1), 129700, DOI: 10.1016/j.cej.2021.129700.

20 E. Garcia-Bordejé, A. M. Benito and W. K. Maser, Graphene aerogels via hydrothermal gelation of graphene oxide colloids: Fine-tuning of its porous and chemical properties and catalytic applications, *Adv. Colloid Interface Sci.*, 2021, **292**, 102420.

21 P. Joshi, O. P. Sharma, S. K. Ganguly, M. Srivastava and O. P. Khatri, Fruit waste-derived cellulose and graphene-based aerogels: Plausible adsorption pathways for fast and efficient removal of organic dyes, *J. Colloid Interface Sci.*, 2022, **608**, 2870–2883, DOI: 10.1016/j.jcis.2021.11.016.

22 M. Hasanpour and M. Hatami, Photocatalytic performance of aerogels for organic dyes removal from wastewaters: Review study, *J. Mol. Liq.*, 2020, **309**, 113094, DOI: 10.1016/j.molliq.2020.113094.

23 M. Wu, J. Liao, L. Yu, R. Lv, P. Li, W. Sun, *et al.*, 2020 Roadmap on Carbon Materials for Energy Storage and Conversion, *Chem.–Asian J.*, 2020, **15**(7), 995–1013.

24 C. Androulidakis, M. Kotsidi, G. Gorgolis, C. Pavlou, L. Sygellou, G. Paterakis, *et al.*, Multi-functional 2D hybrid aerogels for gas absorption applications, *Sci. Rep.*, 2021, **11**(1), 13548, DOI: 10.1038/s41598-021-92957-8.

25 G. Gorgolis, E. Messina, M. Kotsidi, M. P. Staccioli, E. Lesaria Nhuch, G. Di Carlo, *et al.*, Antifungal Graphene-based Absorbers as Advanced Materials for Preventive Conservation of Cultural Objects, *ChemNanoMat*, 2022, **8**(12), e202200265.

26 G. Gorgolis, M. Kotsidi, G. Paterakis, N. Koutroumanis, C. Tsakonas and C. Galiotis, Graphene aerogels as efficient adsorbers of water pollutants and their effect of drying methods, *Sci. Rep.*, 2024, **14**(1), 1–11, DOI: 10.1038/s41598-024-58651-1.

27 A. Kovtun, E. Campodoni, L. Favaretto, M. Zambianchi, A. Salatino, S. Amalfitano, *et al.*, Multifunctional graphene oxide/biopolymer composite aerogels for microcontaminants removal from drinking water, *Chemosphere*, 2020, **259**, 1–10.

28 L. Han, A. M. E. Khalil, J. Wang, Y. Chen, F. Li, H. Chang, *et al.*, Graphene-boron nitride composite aerogel: A high efficiency adsorbent for ciprofloxacin removal from water, *Sep. Purif. Technol.*, 2022, **278**, 119605, DOI: 10.1016/j.seppur.2021.119605.

29 J. Sun, M. Yu, R. Kang, H. Sun, Y. Zhang and N. Wang, Self-assembled graphene aerogels for removal of methylene blue and copper from aqueous solutions, *J. Hazard. Mater. Adv.*, 2021, **4**, 100026, DOI: 10.1016/j.hazadv.2021.100026.

30 T. T. P. N. X. Trinh, D. M. Nguyet, T. H. Quan, T. N. M. Anh, D. B. Thinh, L. T. Tai, *et al.*, Preparing three-dimensional graphene aerogels by chemical reducing method: Investigation of synthesis condition and optimization of

adsorption capacity of organic dye, *Surf. Interfaces*, 2021, **23**, 101023, DOI: **10.1016/j.surfin.2021.101023**.

31 G. Gorgolis, M. Kotsidi, E. Messina, V. M. Miritana, C. G. Di and E. L. Nhuch, Antifungal Hybrid Graphene – Transition-Metal Dichalcogenides Aerogels with an Ionic Liquid Additive as Innovative Absorbers for Preventive Conservation of Cultural Heritage, *Materials*, 2024, 3174.

32 L. Sygellou, G. Paterakis, C. Galiotis and D. Tasis, Work Function Tuning of Reduced Graphene Oxide Thin Films, *J. Phys. Chem. C*, 2016, **120**(1), 281–290.

33 G. Paterakis, E. Vaughan, D. R. Gawade, R. Murray, G. Gorgolis and S. Matsalis, Highly Sensitive and Ultra-Responsive Humidity Sensors Based on Graphene Oxide Active Layers and High Surface Area Laser-Induced Graphene Electrodes, *Nanomaterials*, 2022, 2684.

34 G. Paterakis, G. Anagnostopoulos, L. Sygellou and C. Galiotis, Protection of Aluminum Foils against Environmental Corrosion with Graphene-Based Coatings, *J. Coat. Sci. Technol.*, 2021, **8**, 18–28.

35 B. Saner Okan, A Sustainable and Scalable Method for Graphene Production, *PCT Pat.*, application, PCT/TR2024/050394, 2024.

36 J. Y. Hong, E. H. Sohn, S. Park and H. S. Park, Highly-efficient and recyclable oil absorbing performance of functionalized graphene aerogel, *Chem. Eng. J.*, 2015, **269**, 229–235, DOI: **10.1016/j.cej.2015.01.066**.

37 H. D. Pham, V. H. Pham, T. V. Cuong, T. D. Nguyen-Phan, J. S. Chung, E. W. Shin, *et al.*, Synthesis of the chemically converted graphene xerogel with superior electrical conductivity, *Chem. Commun.*, 2011, **47**(34), 9672–9674.

38 R. Bardestani, G. S. Patience and S. Kaliaguine, Experimental methods in chemical engineering: specific surface area and pore size distribution measurements—BET, BJH, and DFT, *Can. J. Chem. Eng.*, 2019, **97**(11), 2781–2791.

39 D. Liu, Q. Bian, Y. Li, Y. Wang, A. Xiang and H. Tian, Effect of oxidation degrees of graphene oxide on the structure and properties of poly (vinyl alcohol) composite films, *Compos. Sci. Technol.*, 2016, **129**, 146–152, DOI: **10.1016/j.compscitech.2016.04.004**.

40 R. Siburian, H. Sihotang, S. Lumban Raja, M. Supeno and C. Simanjuntak, New route to synthesize of graphene nano sheets, *Orient. J. Chem.*, 2018, **34**(1), 182–187.

41 O. M. Lemine, Microstructural characterisation of α - Fe2O3 nanoparticles using, XRD line profiles analysis, FE-SEM and FT-IR, *Superlattices Microstruct.*, 2009, **45**(6), 576–582, DOI: **10.1016/j.spmi.2009.02.004**.

42 A. C. Ferrari and D. M. Basko, Raman spectroscopy as a versatile tool for studying the properties of graphene, *Nat. Nanotechnol.*, 2013, **8**(4), 235–246, DOI: **10.1038/nnano.2013.46**.

43 A. C. Ferrari, J. C. Meyer, V. Scardaci, C. Casiraghi, M. Lazzeri, F. Mauri, *et al.*, Raman spectrum of graphene and graphene layers, *Phys. Rev. Lett.*, 2006, **97**(18), 1–4.

44 M. Kotsidi, G. Gorgolis, M. G. Pastore Carbone, G. Paterakis, G. Anagnostopoulos, G. Trakakis, *et al.*, Graphene nanoplatelets and other 2D-materials as protective means against the fading of coloured inks, dyes and paints, *Nanoscale*, 2023, 5414–5428.

45 I. Karnis, F. Krasanakis, L. Sygellou, A. N. Rissanou, K. Karatasos and K. Chrissopoulou, Varying the degree of oxidation of graphite: effect of oxidation time and oxidant mass, *Phys. Chem. Chem. Phys.*, 2024, 10054–10068.

46 X. Wu, G. Hong and X. Zhang, Electroless Plating of Graphene Aerogel Fibers for Electrothermal and Electromagnetic Applications, *Langmuir*, 2019, **35**(10), 3814–3821.

47 X. Wang, J. Li, Y. Luo and M. Huang, A Novel Ammonium Perchlorate/Graphene Aerogel Nanostructured Energetic Composite: Preparation and Thermal Decomposition, *Adv. Mater. Sci.*, 2014, **6**(3), 530–537, DOI: **10.1166/sam.2014.1774**.

48 L. Zhou, Z. Yang, J. Yang, Y. Wu and D. Wei, Facile syntheses of 3-dimension graphene aerogel and nanowalls with high specific surface areas, *Chem. Phys. Lett.*, 2017, **677**, 7–12, DOI: **10.1016/j.cplett.2017.03.076**.

49 M. Thommes, K. Kaneko, A. V. Neimark, J. P. Olivier, F. Rodriguez-Reinoso, J. Rouquerol, *et al.*, Physisorption of gases, with special reference to the evaluation of surface area and pore size distribution (IUPAC Technical Report), *Pure Appl. Chem.*, 2015, **87**(9–10), 1051–1069.

50 H. Mahmoodi, M. Fattahi and M. Motevassel, Graphene oxide-chitosan hydrogel for adsorptive removal of diclofenac from aqueous solution: Preparation, characterization, kinetic and thermodynamic modelling, *RSC Adv.*, 2021, **11**(57), 36289–36304, DOI: **10.1039/D1RA06069D**.

51 B. Y. Z. Hiew, L. Y. Lee, K. C. Lai, S. Gan, S. Thangalazhy-Gopakumar, G. T. Pan, *et al.*, Adsorptive decontamination of diclofenac by three-dimensional graphene-based adsorbent: Response surface methodology, adsorption equilibrium, kinetic and thermodynamic studies, *Environ. Res.*, 2019, **168**, 241–253.

52 S. Khaliha, Graphene Based Materials For Water Purification, PhD thesis, University of Bologna, 2024.

53 S. Khaliha, F. Tunioli, L. Foti, A. Bianchi, A. Kovtun, T. D. Marforio, *et al.*, Upcycling of plastic membrane industrial scraps and reuse as sorbent for emerging contaminants in water, *Environ. Sci.: Water Res. Technol.*, 2024, **10**(5), 1097–1107.

54 S. Mantovani, T. D. Marforio, S. Khaliha, A. Pintus, A. Kovtun, F. Tunioli, *et al.*, Amino acid-driven adsorption of emerging contaminants in water by modified graphene oxide nanosheets, *Environ. Sci.: Water Res. Technol.*, 2023, **9**(4), 1030–1040.

55 L. Lonappan, S. K. Brar, R. K. Das, M. Verma and R. Y. Surampalli, Diclofenac and its transformation products: Environmental occurrence and toxicity - A review, *Environ. Int.*, 2016, **96**, 127–138, DOI: **10.1016/j.envint.2016.09.014**.

56 A. M. E. Khalil, F. A. Memon, T. A. Tabish, D. Salmon, S. Zhang and D. Butler, Nanostructured porous graphene for efficient removal of emerging contaminants (pharmaceuticals) from water, *Chem. Eng. J.*, 2020, **398**, 125440.